

Structural atomistic mechanism for the glass transition entropic scenario

Dong Han,^{1,2} Dan Wei,^{1,2} Jie Yang,^{1,2} Hui-Ling Li,^{1,2} Min-Qiang Jiang,^{1,2}
Yun-Jiang Wang,^{1,2,*} Lan-Hong Dai,^{1,2,†} and Alessio Zaccone^{3,4,5,‡}

¹*State Key Laboratory of Nonlinear Mechanics, Institute of Mechanics,
Chinese Academy of Sciences, Beijing 100190, China*

²*School of Engineering Science, University of Chinese Academy of Sciences, Beijing 100049, China*

³*Department of Physics A. Pontremoli, University of Milan, via Celoria 16, 20133 Milan, Italy*

⁴*Cavendish Laboratory, University of Cambridge,*

JJ Thomson Avenue, Cambridge, CB3 0HE United Kingdom

⁵*Statistical Physics Group, Department of Chemical Engineering and Biotechnology,
University of Cambridge, Cambridge, CB3 0AS, United Kingdom*

(Dated: July 9, 2019)

A popular Adam–Gibbs scenario has suggested that the excess entropy of glass and liquid over crystal dominates the dynamical arrest at the glass transition with exclusive contribution from configurational entropy over vibrational entropy. However, an intuitive structural rationale for the emergence of frozen dynamics in relation to entropy is still lacking. Here we study these issues by atomistically simulating the vibrational, configurational, as well as total entropy of a model glass former over their crystalline counterparts for the entire temperature range spanning from glass to liquid. Besides confirming the Adam–Gibbs entropy scenario, the concept of Shannon information entropy is introduced to characterize the diversity of atomic-level structures, which undergoes a striking variation across the glass transition, and explains the change found in the excess configurational entropy. Hence, the hidden structural mechanism underlying the entropic kink at the transition is revealed in terms of proliferation of certain atomic structures with a higher degree of centrosymmetry, which are more rigid and possess less nonaffine softening modes. In turn, the proliferation of these centrosymmetric (rigid) structures leads to the freezing-in of the dynamics beyond which further structural adjustments become highly unfavourable, thus explaining the kink in the configurational entropy at the transition.

The glass transition is generally regarded as the phenomenon in which a viscous liquid circumvents crystallization and evolves continuously into a disordered solid state directly during fast cooling [1–5]. It is a typical example of the falling-out-of-equilibrium phenomenon that occurs for almost any system the relaxation time of which surpasses laboratory time scales [6]. Considerable efforts have been made to rationalize the glass transition phenomenon, especially those linking it explicitly to the thermodynamics of glass-forming systems. Among them, Gibbs and DiMarzio proposed a classic entropic scenario of glass transition in which the glass state below the glass transition temperature, T_g , is frozen in a single configuration, while the equilibrium liquid above T_g is free to explore all possible high-dimensional configurations [7]. In this description, the excess entropy of glass and liquid over crystal is supposed to originate entirely from the configurational entropy which governs the relaxation timescale. This formulation lays a robust foundation for the well-known Adam–Gibbs relationship, which provides a suggestive connection between dynamics and thermodynamics of glass transition, i.e., time and entropy [8–13].

Subsequently, an energetic description of glass transition and relaxation was motivated by this classic description. The concept of potential energy surface was originally conceived by Goldstein [14], and then Stillinger and Debenedetti developed it into the potential energy

landscape (PEL) theory [2]. In this theory, the configurational space is separated into distinct local potential energy minima (the inherent structures), and the low temperature dynamics is featured by the non-equilibrium evolution of the inherent structures along complex pathways that connect adjacent basins [15, 16]. However, Goldstein argued that atomic or molecular vibrations also contribute to the excess entropy. It is assumed that the vibrational entropy is in a relation of linear response with temperature [17]. A recent computer simulation also revealed that the ideal glass state is not only vibrational [18]. To validate the entropic scenario, contributions to the excess entropy from both vibration and configuration have been evaluated for molecular and network glasses [19, 20], as well as computer Lennard-Jones liquids [21, 22]; however, there are only very few reports on metallic glass-forming systems available in the literature.

It is the lack of thermodynamic stability of supercooled liquids against crystallization in experiments that hinders separating the vibrational and configurational entropy across the glass transition. Recently, Smith *et al.* have successfully obtained the phonon density of states (DOS) thanks to the advances in neutron flux and instrument efficiency for inelastic neutron scattering (INS), which enables capture of vibrational states in a very short time window feasible above T_g , rather than rapid crystallization of the supercooled liquid [23]. Based on these

experiments, the Adam–Gibbs relationship is well corroborated around the glass transition, which indicates vibrational entropy is trivial against its configurational counterpart.

Nevertheless, an entropic picture including fully atomic information in the entire temperature space is missing. As a result, a question naturally arises about which atomic-level structures change the most across the transition [5, 24, 25]. While there exist some hints which may be recognized as structural signatures of glass transition [26–29], an explicit link between structural mechanism and configurational entropy for the dynamical arrest is still missing [5, 24, 25, 30].

Here we fill this gap by disentangling the specific contributions of vibrational and configurational entropy in glass transition and by relating the configurational entropy to the distribution of atomic-level structures. The results may provide a first fully atomistic verification of the Adam–Gibbs scenario. Through introduction of a Shannon information entropy measure of local structural diversity, we rationalize the structural mechanism for the glass transition which is responsible for the variation in configurational entropy. The resulting scenario also offers the unprecedented opportunity of linking entropy, structure and mechanical properties into a single unifying framework.

All the molecular dynamics (MD) simulations are performed by LAMMPS code [31] on a prototypical binary $\text{Cu}_{50}\text{Zr}_{50}$ glass-forming liquid which has been widely studied in simulations, as well as the aforementioned INS experiments [23]. The force field is described by a Finnis–Sinclair type embedded-atom method (EAM) potential [32]. A model simulation box containing 10,976 atoms with dimensions $\sim 60 \times 60 \times 60 \text{ \AA}^3$ is used for estimating the phonon density of states. A bigger simulation box with 31,250 atoms is adopted for studying the structural motifs and their statistical occurrence. The glass sample is prepared by quenching an equilibrium liquid at 2000 K to 0 K with a cooling rate of 10^{10} K/s . A constant temperature, pressure and atom number ensemble is used for both cooling and heating. According to Cu–Zr binary phase diagram [33], multiple crystalline phases are considered as references for the noncrystalline counterparts, i.e., a mixture of orthorhombic $\text{Cu}_{10}\text{Zr}_7$ and Laves CuZr_2 phases at 0 K–988.15 K, and a B2 $\text{Cu}_{50}\text{Zr}_{50}$ phase at 988.15 K–1208.15 K. A conjugate gradient algorithm brings the systems rapidly to their energy minima. Through Intel Math Kernel Library and ARPACK, we diagonalize the Hessian matrix based on the EAM formulation to obtain the vibrational normal modes [34–36]. Then the phonon DOS is obtained in a standard way as $D(\omega) = \frac{1}{3N-3} \sum_{l=1}^{3N-3} \delta(\omega - \omega_l)$, with N being the number of atoms, l the number of vibrational modes, and ω the eigenfrequency. Finally, the local structure motifs of inherent structures are categorized by the Voronoi tessellation. A standard four digit descriptor $\langle n_3, n_4, n_5, n_6 \rangle$ is

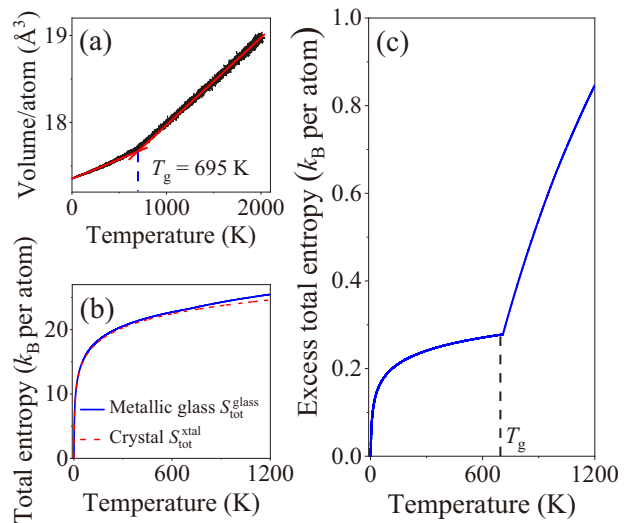


FIG. 1. Glass transition and excess total entropy. (a) Temperature dependence of the volume of a glass-forming liquid during cooling, the discontinuity in slope indicates the glass transition temperature, $T_g = 695 \text{ K}$. (b) Temperature dependence of total entropy in disordered phase and crystal. (c) Temperature dependence of excess total entropy ΔS_{tot} .

used to label a Voronoi polyhedron, where n_i is the number of facets with i edges around a central atom [37, 38].

To quantitatively decouple the specific roles of vibrational entropy S_{vib} and of configurational entropy S_{conf} across the glass transition, we treat the total entropy as $S_{\text{tot}} = S_{\text{vib}} + S_{\text{conf}}$, which can be obtained by thermodynamic integration after heating a glass to liquid, i.e.,

$$S_{\text{tot}} = \int_0^T \frac{dQ}{T} = \int_0^T \frac{dU}{T} (P = 0). \quad (1)$$

Here T is temperature, Q is the absorption heat, U is internal energy, and P is pressure. Figure 1 shows the variation of thermodynamic quantities as temperature involves. In Fig. 1(a), the glass transition is clearly signaled at $T_g = 695 \text{ K}$ by a kink of the volume-temperature curve. The total entropy of glass and crystal over their 0 K reference is displayed in Fig. 1(b) from 0 K to 1200 K. Note that the total entropy of crystal at [0 K, 988.15 K] is assessed by the weighted mean of $\text{Cu}_{10}\text{Zr}_7$ and CuZr_2 phases. One may notice that the total entropy diverges around glass transition. To further quantify this feature, we plot the excess total entropy, ΔS_{tot} , of glass and liquid over crystal in Fig. 1(c). ΔS_{tot} is defined as

$$\Delta S_{\text{tot}} = S_{\text{tot}}^{\text{glass}} - S_{\text{tot}}^{\text{xtal}}. \quad (2)$$

In the following, the symbol Δ denotes the difference between glass (liquid) and crystal in a specific physical quantity. It is noted in Fig. 1(c) that the excess total entropy exhibits two kinks in the whole temperature range. The first one at low temperature is due to a change in vibrational entropy, which will be explained later in detail.

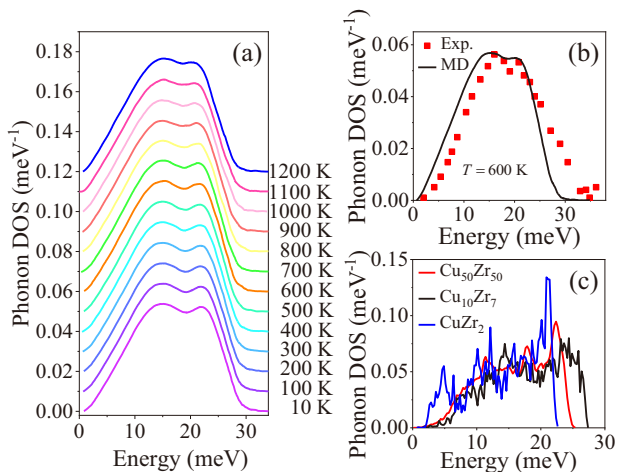


FIG. 2. Phonon of glass-forming liquid and crystal. (a) Phonon DOS of glass and liquid over wide temperature range. (b) Comparison of phonon DOS between simulation and experiment at 600 K. (c) Phonon DOS of three crystal phases including orthorhombic $\text{Cu}_{10}\text{Zr}_7$, Laves CuZr_2 , and B2 $\text{Cu}_{50}\text{Zr}_{50}$.

With respect to the second kink at higher T , it coincides with the glass transition temperature where the excess entropy experiences a significant increase, consistent with the Adam–Gibbs entropic scenario [8].

As for the vibrational entropy, we calculate the phonon DOS of both glass (liquid) and crystals as shown in Fig. 2. The phonon DOSs are calculated over a wide temperature range spanning from far below to far above the glass transition. The data are displayed in Fig. 2(a) for selected temperatures from 10 K to 1200 K. To calibrate the simulations, we also compare the numerical data with INS experimental measurement of phonon at 600 K, as shown in Fig. 2(b). Although MD overestimates the soft modes and underestimates the high-frequency vibration, the simulations are overall comparable to the experiment. The extra soft modes in simulations are from the model preparation with an extremely high cooling rate due to the notoriously limited timescale in MD. For crystals, the vibrational DOSs of $\text{Cu}_{50}\text{Zr}_{50}$, $\text{Cu}_{10}\text{Zr}_7$ and CuZr_2 are all shown in Fig. 2(c), accounting for the different thermodynamically stable crystalline phases at different temperatures.

The vibrational entropy can be calculated from the DOS in a standard way via [23, 39]

$$S_{\text{vib}}(T) = 3k_{\text{B}} \int_0^{\infty} g(E) \{ [1 + n(T)] - \ln [1 + n(T)] - n(T) \ln n(T) \} dE. \quad (3)$$

Here $n(T) = \{\exp[E/(k_{\text{B}}T)] - 1\}^{-1}$ is the Bose-Einstein occupation number with k_{B} the Boltzmann constant. $g(E)$ is the normalized phonon DOS and $E = \hbar\omega_l$ is the phonon energy. The calculated vibrational entropy versus temperature is shown in Fig. 3(a-b) for both

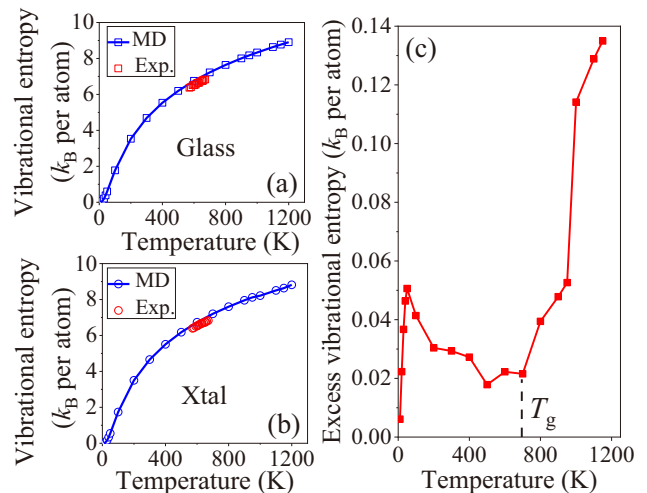


FIG. 3. Vibrational entropy of (a) glass-forming liquid, and (b) crystal as a function of temperature. The simulations are calibrated to the experiments. (c) Temperature dependence of excess vibrational entropy of glass and liquid over crystal.

glass and crystals. It is seen that our calculations agree quantitatively with experiments. The vibration entropies evolve continuously from glass to liquid without any noticeable discontinuity. The excess vibrational entropy of glass (liquid) over crystal $\Delta S_{\text{vib}} = S_{\text{vib}}^{\text{glass}} - S_{\text{vib}}^{\text{xtal}}$ is further plotted in Fig. 3(c), which exhibits two kinks in analogy with the excess total entropy; see Fig. 1(c).

Once one has the excess total entropy ΔS_{tot} and the excess vibrational entropy ΔS_{vib} , the exact role of configurational entropy

$$\Delta S_{\text{conf}} = \Delta S_{\text{tot}} - \Delta S_{\text{vib}} \quad (5)$$

played in glass transition can be examined by subtracting the vibrational part from the total entropy. The excess entropy of glass (liquid) over crystal is summarized in Fig. 4 over the entire temperature range, which includes the temperature observation window of the experiments. The excess vibrational entropy is trivial in most of the temperature range compared with configurational entropy. The striking variation in excess entropy near the glass transition is mainly from the change in configurational entropy, whereas the vibrational entropy varies moderately at the transition. Such data unambiguously support the Adam–Gibbs entropy scenario and is consistent with experimental observations [23].

The bare configurational entropy is further shown in the inset of Fig. 5(d) to clearly confirm its critical role in the glass transition. However, at low temperature, there is also a comparable contribution to the excess total entropy from vibrations, since the inherent structure does not evolve at all. Even though the configurational entropy remains unchanged, the vibrational entropy is more sensitive to temperature and should increase markedly at the very beginning of heating at 0 K; see Fig. 3(c).

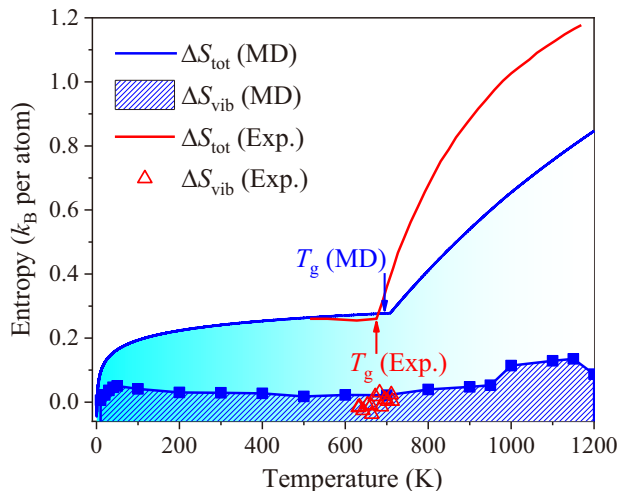


FIG. 4. Panorama of excess total and vibrational entropy over entire temperature range. The excess total entropy experiences abrupt increase upon glass transition with dominating contribution from its configurational component. The simulations are calibrated by experiments.

Physically, the entropy from dynamical sources increases as temperature goes up because the system explores a larger volume in the phase space with stronger excitations of dynamical degrees of freedom [39]. Finally, we note that T_g in simulations is a bit higher than that found in experiments. The slight difference is understandable since the MD model is being quenched much faster, which makes the inherent structure remain on higher positions in the PEL.

Now that we have tested the validity of the Adam–Gibbs scenario, the remaining unsolved issue is whether there is any unambiguous structural variation that is linked with the evolution of the configurational entropy. This link is crucial to explain the variation in linear response to external fields such as shear, which is deeply rooted in the microstructure [40]. However, if one cares only about the structure at the level of two-body correlation, or the fraction of a specific local structure, usually there is no dramatic change accounting for the dynamical arrest. To figure out the hidden variables, the Voronoi tessellation scheme is adopted to analyze the inherent structures [37, 38].

The distributions of the 30 most frequent Voronoi polyhedra are displayed in Fig. 5(a) for both glass and liquid. Although the geometries of the clusters do not change much from liquid to glass, their distribution does change as evidenced by the difference, ΔP_i , of fractions at 1200 K and 10 K, respectively. The geometric structures that are most frequent in the deep glass state become less populated in the liquid state upon crossing the glass transition. Consequently, the local structures in the liquid are more evenly distributed, which in turn increases the diversity of structures and the corresponding configurational en-

trophy. In order to compare with disordered states, we also list the local structures of the three crystalline phases in Fig. 5(b). Only very few local structures are present in crystals, indicating very low configurational entropy.

In order to further quantify the diversity of structures and the configurational entropy, we introduce the concept of Shannon information entropy [41] associated with the incidence of local Voronoi structures (polyhedra) in disordered liquid and glass states [42], which reads

$$S_{\text{Shannon}} = - \sum_{i=1}^n P_i(x_i) \ln P_i(x_i), \quad (6)$$

here $P(x_i)$ is the normalized probability density of a Voronoi polyhedron x_i . The Shannon entropy provides a “solid and quantitative basis for the interpretation of the thermodynamic entropy” [43], and here we use it as a qualitative measure for the evolution of the configurational entropy in the physical system.

The computed the Shannon entropy of glass-forming systems is shown in Fig. 5(c). It is seen that the Shannon entropy rises abruptly at the glass transition temperature, which is signaled by a kink. As Fig. 5(d) demonstrates, the variation of excess configurational entropy ΔS_{conf} (Eq. (5)) is in very good qualitative agreement with the change in Shannon entropy $\Delta S_{\text{Shannon}}$. This is not a coincidence but a strong evidence that the change of diversity in local atomic structures yields an abrupt rise of configurational entropy as suggested in the Adam–Gibbs entropic scenario. However, if one examines the temperature dependence of a specific local structure, e.g., $\langle 0, 3, 6, 4 \rangle$, as shown in Fig. 5(c), there is no critical change. Thus, we do find a hidden structural change across the glass transition from a statistical perspective, which has been puzzling for decades. For a first approximation, we deduce the Kauzmann temperature as $T_K = 590$ K by extrapolating the excess configurational entropy to zero, which is supported by the experimental data, such as $T_K = 571$ K in Ref. [44], and $T_K = 627$ K in Ref. [23]. Finally, we note that a larger model with 31,250 atoms is applied for the Voronoi structure analysis. As seen in Fig. S1 [45], such model size yields nearly converged diversity of local Voronoi structures.

The increase of the fraction of *certain* geometrically favoured local structures upon lowering the temperature is also linked to an increase of local centrosymmetry [46], as demonstrated by the evolution of the average non-centrosymmetry parameter defined in [47], as shown in Fig. S2 [45]. Hence, the configurationally favored structures turn out to coincide with those that are more centrosymmetric and thus more rigid [46], which gives higher rigidity to the system and a lower boson peak (lower soft modes) [46, 48]. In terms of both Voronoi polyhedra and entropies, a natural link between entropy and rigidity/elasticity of glass-forming systems can thus be established. Therefore, the present results may lead to a uni-

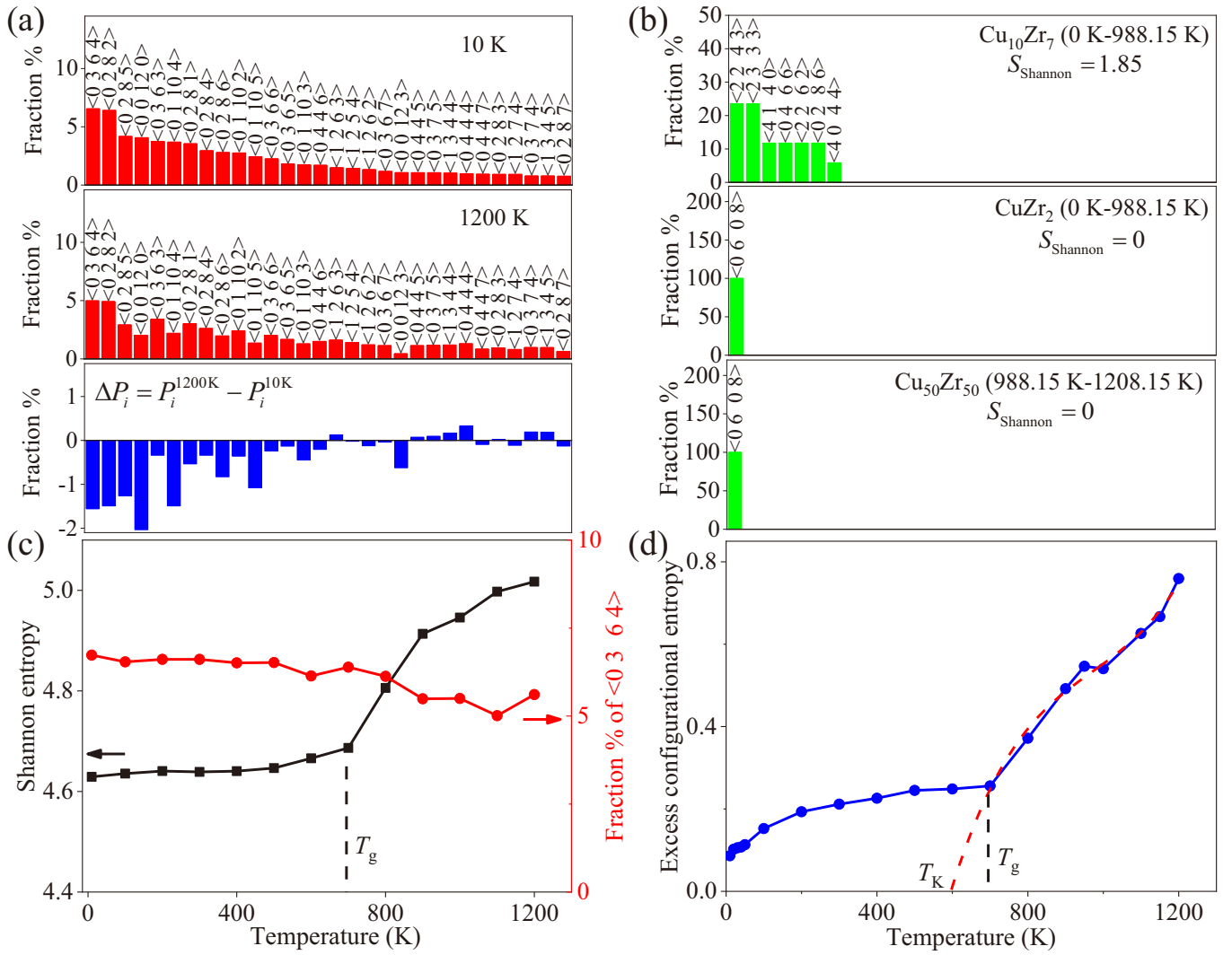


FIG. 5. Shannon entropy of local structures across the glass transition as a microscopic measure of configurational entropy. (a) Distribution and variation of 30 most frequent Voronoi polyhedra at 10 K and 1200 K, respectively. (b) Distribution of Voronoi polyhedra in crystals. (c) Temperature dependence of Shannon entropy which is extracted from the distribution of local structures. The fraction of a specific Voronoi polyhedron $\langle 0, 3, 6, 4 \rangle$ is shown for comparison. (d) Temperature dependence of excess configurational entropy of glass-forming liquid, which is extracted from the difference between total entropy and the vibrational entropy as plotted in Fig. 4.

fication of apparently different concepts of glass transition, i.e., entropy in the Adam–Gibbs sense [8], the shear modulus in the shoving-model [3, 6, 10, 49] and Frenkel’s viscoelastic crossover [50, 51].

In conclusion, our results provide microscopic insights into the Adam–Gibbs entropic scenario of the glass transition in a model atomic glass former via quantification of temperature-dependent total, vibrational, and configurational entropies. The change of entropy that dominates the glass transition is confirmed to be originated mostly from configurational entropy while the vibrational entropy is featureless at the transition. The findings are in agreement with recent INS experiments, and independent simulations [52] and provide additional atomistic

details. The hidden emergence of atomic-level structures leading to dynamical arrest is unambiguously revealed by studying the distributions of local Voronoi polyhedra in terms of Shannon information entropy. In particular, upon decreasing T in the liquid it is seen that a limited number of Voronoi polyhedra become more frequent with respect to all the others, which makes the distribution of Voronoi polyhedra more uneven and thus reduces the configurational and Shannon entropies. Since the favoured polyhedra are associated with a higher degree of local centrosymmetry, hence with mechanical rigidity (they have less nonaffine softening modes [46]) this eventually leads to a rigidification process at the glass transition, after which further structural adjustments become

energetically unfavourable due to the rigid environment and the configurational entropy then decreases much less with further decreasing T in the solid glass.

The emerging scenario may pave the way for constructing a complete framework eventually connecting structure, entropy and viscoelasticity at the glass transition of liquids.

This work is supported by the NSFC (No. 11672299 and No. 11790292), and the National Key Research and Development Program of China (No. 2017YFB0702003 and No. 2017YFB0701502); the Strategic Priority Research Program (No. XDB22040303), the Key Research Program of Frontier Sciences (No. QYZDJSSW-JSC011), and the Youth Innovation Promotion Association of Chinese Academy of Sciences (No. 2017025). Useful discussions with Stefano Martiniani are gratefully acknowledged.

* yjwang@imech.ac.cn

† lhdai@lnm.imech.ac.cn

‡ az302@cam.ac.uk

- [1] C. A. Angell, *Science* **267**, 1924 (1995).
- [2] P. G. Debenedetti and F. H. Stillinger, *Nature* **410**, 259 (2001).
- [3] J. C. Dyre, *Rev. Mod. Phys.* **78**, 953 (2006).
- [4] J. S. Langer, *Reports Prog. Phys.* **77**, 042501 (2014).
- [5] C. P. Royall and S. R. Williams, *Phys. Rep.* **560**, 1 (2015).
- [6] J. C. Dyre, *Phys. Today* **61**, 15 (2008).
- [7] J. H. Gibbs and E. A. DiMarzio, *J. Chem. Phys.* **28**, 373 (1958).
- [8] G. Adam and J. H. Gibbs, *J. Chem. Phys.* **43**, 139 (1965).
- [9] L.-M. Martinez and C. A. Angell, *Nature* **410**, 663 (2001).
- [10] J. C. Dyre, T. Hechsher, and K. Niss, *J. Non-Cryst. Solids* **355**, 624 (2009).
- [11] J. C. Dyre, *J. Chem. Phys.* **149**, 210901 (2018).
- [12] F. W. Starr, J. F. Douglas, and S. Sastry, *The Journal of Chemical Physics* **138**, 12A541 (2013), <https://doi.org/10.1063/1.4790138>.
- [13] L. Berthier and G. Biroli, *Rev. Mod. Phys.* **83**, 587 (2011).
- [14] M. Goldstein, *J. Chem. Phys.* **51**, 3728 (1969).
- [15] S. Sastry, P. G. Debenedetti, and F. H. Stillinger, *Nature* **393**, 554 (1998).
- [16] Y. Fan, T. Iwashita, and T. Egami, *Nat. Commun.* **8**, 15417 (2017).
- [17] M. Goldstein, *J. Chem. Phys.* **64**, 4767 (1976).
- [18] M. Ozawa, A. Ikeda, K. Miyazaki, and W. Kob, *Phys. Rev. Lett.* **121**, 205501 (2018).
- [19] P. Gujrati and M. Goldstein, *J. Phys. Chem.* **84**, 859 (1980).
- [20] G. Johari, *J. Chem. Phys.* **112**, 7518 (2000).
- [21] F. Sciortino, W. Kob, and P. Tartaglia, *Phys. Rev. Lett.* **83**, 3214 (1999).
- [22] M. Ozawa, G. Parisi, and L. Berthier, *J. Chem. Phys.* **149**, 154501 (2018).
- [23] H. L. Smith, C. W. Li, A. Hoff, G. R. Garrett, D. S. Kim, F. C. Yang, M. S. Lucas, T. Swan-Wood, J. Y. Y. Lin, M. B. Stone, D. L. Abernathy, M. D. Demetriou, and B. Fultz, *Nat. Phys.* **13**, 900 (2017).
- [24] H. Tong and H. Tanaka, *Phys. Rev. X* **8**, 011041 (2018).
- [25] H. Tanaka, H. Tong, R. Shi, and J. Russo, *Nat. Rev. Phys.* **1**, 333 (2019).
- [26] Y. T. Shen, T. H. Kim, A. K. Gangopadhyay, and K. F. Kelton, *Phys. Rev. Lett.* **102**, 057801 (2009).
- [27] J. Ding, Y.-Q. Cheng, H. Sheng, and E. Ma, *Phys. Rev. B* **85**, 060201 (2012).
- [28] Y. Hu, F. Li, M. Li, H. Bai, and W. Wang, *Nat. Commun.* **6**, 8310 (2015).
- [29] S. S. Schoenholz, E. D. Cubuk, D. M. Sussman, E. Kaxiras, and A. J. Liu, *Nat. Phys.* **12**, 469 (2016).
- [30] C. Patrick Royall, S. R. Williams, T. Ohtsuka, and H. Tanaka, *Nat. Mater.* **7**, 556 (2008).
- [31] S. Plimpton, *J. Comput. Phys.* **117**, 1 (1995).
- [32] M. Mendeleev, M. Kramer, R. Ott, and D. Sordelet, *Philos. Mag.* **89**, 109 (2009).
- [33] D. Arias and J. P. Abriata, *Journal of Phase Equilibria* **11**, 452 (1990).
- [34] A. Widmer-Cooper, H. Perry, P. Harrowell, and D. R. Reichman, *Nat. Phys.* **4**, 711 (2008).
- [35] H. Shintani and H. Tanaka, *Nat. Mater.* **7**, 870 (2008).
- [36] J. Ding, Y.-Q. Cheng, H. Sheng, M. Asta, R. O. Ritchie, and E. Ma, *Nat. Commun.* **7**, 13733 (2016).
- [37] H. W. Sheng, W. K. Luo, F. M. Alamgir, J. M. Bai, and E. Ma, *Nature* **439**, 419 (2006).
- [38] Y. Cheng and E. Ma, *Prog. Mater. Sci.* **56**, 379 (2010).
- [39] B. Fultz, *Prog. Mater. Sci.* **55**, 247 (2010).
- [40] E. D. Cubuk, R. J. S. Ivancic, S. S. Schoenholz, D. J. Strickland, A. Basu, Z. S. Davidson, J. Fontaine, J. L. Hor, Y.-R. Huang, Y. Jiang, N. C. Keim, K. D. Koshigan, J. A. Lefever, T. Liu, X.-G. Ma, D. J. Magagnosc, E. Morrow, C. P. Ortiz, J. M. Rieser, A. Shavit, T. Still, Y. Xu, Y. Zhang, K. N. Nordstrom, P. E. Arratia, R. W. Carpick, D. J. Durian, Z. Fakhraai, D. J. Jerolmack, D. Lee, J. Li, R. Riggelman, K. T. Turner, A. G. Yodh, D. S. Gianola, and A. J. Liu, *Science* **358**, 1033 (2017).
- [41] C. E. Shannon, *Bell System Technical Journal* **27**, 379 (1948).
- [42] D. Wei, J. Yang, M.-Q. Jiang, L.-H. Dai, Y.-J. Wang, J. C. Dyre, I. Douglass, and P. Harrowell, *J. Chem. Phys.* **150**, 114502 (2019).
- [43] A. Ben-Naim, *Entropy* **19** (2017), 10.3390/e19020048.
- [44] T. Wang, T. E. Cullinan, and R. E. Napolitano, *Acta Mater.* **62**, 188 (2014).
- [45] See Supplemental Material at xxx for details of calculations, sample size dependence of Shannon entropy, and non-centro-symmetry parameter.
- [46] R. Milkus and A. Zaccone, *Phys. Rev. B* **93**, 094204 (2016).
- [47] C. L. Kelchner, S. J. Plimpton, and J. C. Hamilton, *Phys. Rev. B* **58**, 11085 (1998).
- [48] J. Yang, Y.-J. Wang, E. Ma, A. Zaccone, L. H. Dai, and M. Q. Jiang, *Phys. Rev. Lett.* **122**, 015501 (2019).
- [49] J. Krausser, K. H. Samwer, and A. Zaccone, *Proceedings of the National Academy of Sciences* **112**, 13762 (2015), <https://www.pnas.org/content/112/45/13762.full.pdf>.
- [50] K. Trachenko and V. V. Brazhkin, *Scientific Reports* **3**, 2188 EP (2013), article.
- [51] K. Trachenko and V. V. Brazhkin, *Reports on Progress in Physics* **79**, 016502 (2016), [arXiv:1512.06592](https://arxiv.org/abs/1512.06592) [cond-mat.soft].

- [52] R. Alvarez-Donado and A. Antonelli, arXiv e-prints , arXiv:1907.02611 (2019), [arXiv:1907.02611 \[cond-mat.soft\]](#).